Controlled Doping of Silicon Nanocrystals Investigated by Solution-Processed Field Effect Transistors

Ryan Gresback,[†] Nicolaas J. Kramer,[‡] Yi Ding,[†] Ting Chen,[§] Uwe R. Kortshagen,[‡,*] and Tomohiro Nozaki[†,*]

[†]Department of Mechanical Science and Engineering, Graduate School of Science and Engineering, Tokyo Institute of Technology, 2-12-1 Ookayama, Meguro-ku, Tokyo 152-8552, Japan, [‡]Department of Mechanical Engineering, University of Minnesota, 111 Church Street SE, Minneapolis, Minnesota 55455, United States, and [§]Department of Chemical Engineering and Materials Science, University of Minnesota, 421 Washington Avenue SE, Minneapolis, Minnesota 55455, United States

ABSTRACT The doping of semiconductor nanocrystals (NCs), which is vital for the optimization of NC-based devices, remains a significant challenge. While gas-phase plasma approaches have been successful in incorporating dopant atoms into NCs, little is known about their electronic activation. Here, we investigate the electronic properties of doped silicon NC thin films cast from solution by field effect transistor analysis. We find that, analogous to bulk silicon, boron and phosphorus electronically dope Si NC thin films; however, the dopant activation efficiency is only $\sim 10^{-2}$–10^{-4}. We also show that surface doping of Si NCs is an effective way to alter the carrier concentrations in Si NC films.

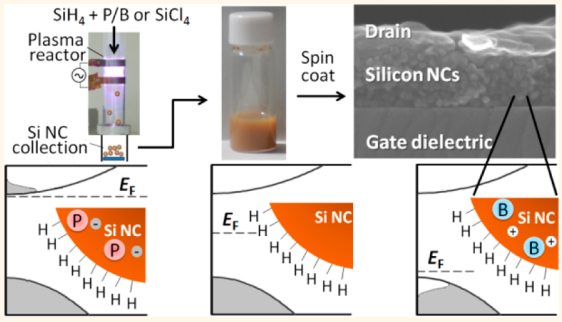

KEYWORDS: silicon · nanocrystal · field effect transistor · dopants · phosphorus · boron

Semiconductor nanocrystals (NCs) are of great interest for a variety of optoelectronic applications, including light-emitting devices[1] and photovoltaics[2] where the control or tunability of carrier transport is crucial to device operation. In order to further tune the electronic and optical properties of NCs, the intentional inclusions of impurities, or dopants, has received significant attention to increase the performance of devices by controlling the number of carriers and by altering the Fermi level in NC films.[3]

Synthesis of impurity-doped NCs is especially challenging for colloidal synthesis techniques,[3,4] and it has only recently become possible to dope CdSe[5−7] and PbSe[8,9] NCs. Doping during gas-phase synthesis appears to be easier. For instance, the simple addition of impurities (P or B) in the gas precursor results in inclusion of the dopants that reside in the core of plasma-synthesized Si NCs at an incorporation efficiency of about 10%.[10,11] However, all of these incorporated dopants are not necessarily electronically activated.

The emergence of localized surface plasmon resonances (LSPRs) at very high dopant concentrations in oxide-free Si NCs, synthesized with the same system as this study, suggests that only a small fraction of the dopants in the core are electronically active.[12] This is consistent with earlier studies of gas-phase-synthesized powders of surface-oxidized, P-doped Si NCs, where only 10^{-3} to 10^{-4} of the nominal P concentration were determined by EPR to be electronically active.[11]

While a limited number of studies has focused on the carrier mobility in Si NC thin films,[14−16] to our knowledge, no study has investigated the dopant activation efficiency in carefully prepared films of electronically coupled doped Si NCs. Thin-film field effect transistors (FETs) are particularly useful in providing information about the mobility of carriers and the Fermi level of NC films.[5,8,13]

Here, we report, to our knowledge, the first study that uses FET measurements to investigate the carrier mobility and Fermi level of B- and P-doped Si NC FETs. Comparison with the nominal dopant concentration enables us to derive the dopant activation efficiency in Si NCs in a functional electronic

* Address correspondence to kortshagen@umn.edu; tnozaki@mech.titech.ac.jp.

Received for review January 11, 2014 and accepted May 15, 2014.

Published online May 15, 2014
10.1021/nn500182b

film. We investigate two sizes of Si NCs, namely, large (8−15 nm) and small (4−7 nm), to elucidate potential size-dependent effects.

Finally, the observation of LSPR in chlorine-terminated Si NCs,[17] which are otherwise undoped, in contact with certain solvents suggests that the surface termination of Si NCs can cause effective surface doping. Hence, we also examine the role of hydrogen and chlorine surface termination in doping of Si NCs.

RESULTS AND DISCUSSION

Si NC suspensions ("inks") are produced by the addition of solvent (1,2-dichlorobenezene, DCB) to free-standing B- and P-doped Si NCs produced using a nonthermal plasma process, which has been described elsewhere,[10,18,19] followed by ultrasonication. The nominal concentration of dopants is defined as $N_{a,nom} = n_{Si}[PH_3]/([SiH_4] + [PH_3])$ or $2N_{a,nom} = n_{Si}[B_2H_6]/([SiH_4] + [B_2H_6])$, where $[PH_3]$, $[SiH_4]$, and $[B_2H_6]$ are the number of phosphine, silane, and diborane molecules introduced to the plasma, respectively, and n_{Si} is the atomic density of silicon (5×10^{22} cm^{-3}). The Si NC suspensions used in this study appear cloudy but stable over long periods of time (days to months). Figure 1a shows a photograph of a Si NC suspension in DCB and an overview of some main steps for Si NC thin-film FET fabrication.

Si NC thin films fabricated by successive spin-coating are observed to be closely packed and form a continuous film over the entire substrate without cracks. Figure 1b shows a cross-sectional SEM image of a Si NC thin-film FET fabricated from large NCs, with diameters of 8−15 nm (see Supporting Information Figure S1 for SEM images comparing small NCs and large NC FETs). The Si NC thin films typically have about 2−5 monolayers of thickness variation, with a few large (order of 100's of nm) agglomerates. Figure 1c shows an optical image of a device with the Si NC layer partially removed to show the difference in color between the gate oxide (blue) and Si NC film (golden). The golden color of the thin films corresponds to a thickness of ∼10−40 nm and transitions to different colors with increasing thickness, for example, pink at ∼40−80 nm and green-blue at ∼80−120 nm, due to thin-film interference effects. Typical transmission electron microscope (TEM) images of the large (8−15 nm) and small (4−7 nm) Si NCs are shown in Figure 1d,e (Figure S2 shows X-ray diffraction data of small and large NCs). As previously described, Si NCs synthesized with a nonthermal plasma can be highly crystalline by properly selecting plasma parameters.[11,17−19]

Doped Si NC FET Characteristics. Figure 2 shows typical drain-current (I_D)−gate-voltage (V_{GS}) characteristics for intrinsic and doped Si NC thin films made with large and small NCs. For devices made with nominally low (less than ∼1%) dopant concentrations, n-type behavior is observed. For films fabricated from nominally high P and B concentrations (∼10%), FETs show minimal to no gating behavior, as would be expected for

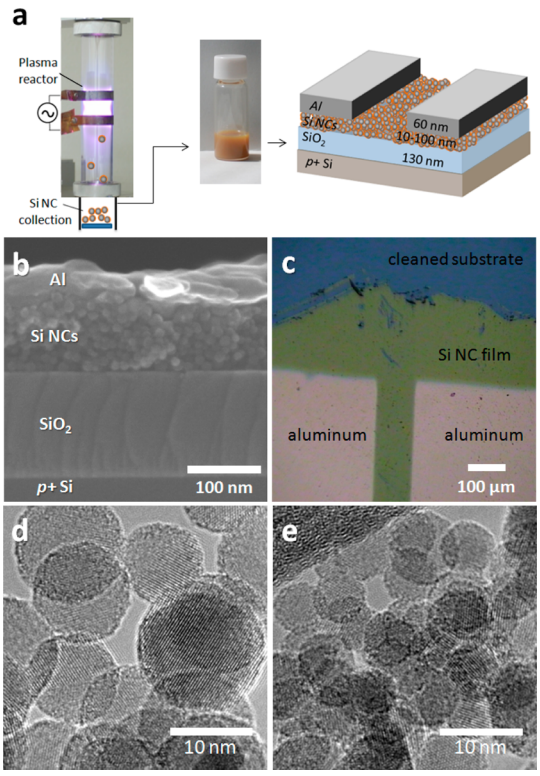

Figure 1. (a) Si NC fabrication process with photographs of a plasma reactor and a suspension of Si NCs in DCB and device structure. (b) SEM cross-sectional image of a device showing layers, from bottom to top, of p+ silicon gate, 130 nm oxide, ∼100 nm Si NC layer, and 60 nm aluminum. (c) Photograph of a Si NC FET with NC layer partially removed to expose blue oxide. The golden color corresponds to the Si NC thin films (∼30 nm), and gray to the aluminum source and drain top contacts. TEM images of (d) large (8−15 nm) and (e) small (4−7 nm) Si NCs.

degenerately doped Si, where the heavily doped Si NCs approach the metallic regime. The trace for nominally 10% B large Si NCs shows a slight decrease in I_D with increasing V_{GS}, while the trace for nominally 10% P large Si NCs shows nearly constant current. Importantly, the threshold voltage (V_T), where the device "turns on", is observed to be strongly dependent on the doping type and concentration. This is clearly shown in Figure 2b, where the traces have been normalized for variations in the mobility.

Figure 2 also shows the difference between fast (10 V s^{-1}) and slow (1 V s^{-1}) sweep rates of the gate voltage (V_{GS}). For slow sweep rates, a significant hysteresis is observed along with lower "off" currents, while for fast sweep rates the hysteresis is significantly reduced, but off-currents can be significant. The observed hysteresis is attributed to screening of carriers caused by traps, likely at the gate-oxide/NC interface or NC surface,[20,21] and the creation or removal of defects related to silicon-hydride species.[22,23] A more detailed discussion on this hysteresis and other transient processes in Si NCs films is available in the Supporting Information. For nominally low doped Si NCs the on/off ratio varied between 10^1 and 10^4, where the off-current was also dependent on NC film thickness

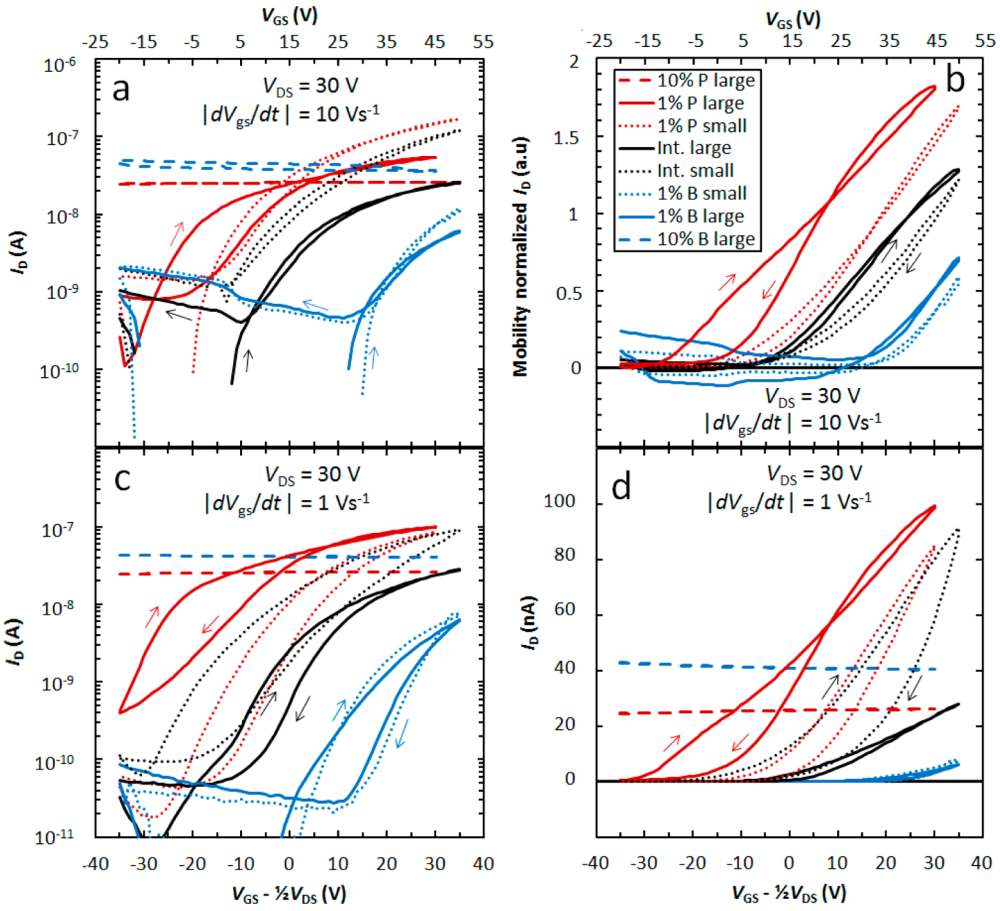

Figure 2. Drain-current (I_D)−gate-voltage (V_{GS}) characteristics of doped Si NC thin-film FETs (a) measured using a fast sweep rate of 10 V s^{-1} for (red) P- and (blue) B-doped (dashed) 10% 8−15 nm, (solid) 1% 8−15 nm, (dot) 1% 4−7 nm, (black solid) intrinsic 8−15 nm, and (black dot) intrinsic 4−7 nm Si NCs, (b) mobility-normalized I_D−V_{GS} characteristics plotted on a linear scale, and the same devices measured with a slower sweep rate of 1 V s^{-1} on (c) a semilog scale and (d) a non-normalized linear scale. All devices shown have a width/length (W/L) of 2000/20 μm and are measured with a drain-source voltage (V_{DS}) of 30 V.

(see Supporting Information Figures S3) and the aforementioned sweep rate of V_{GS}.

From the I_D−V_{GS} traces the threshold voltage (V_T) and the linear mobility (μ_{lin}) can be determined as the x-intercept and slope of the linear region, respectively, based on the gradual channel approximation:[24]

$$I_D = (W/L)C_{ox}\mu_{lin}\left[V_{GS} - \left(\frac{1}{2}V_{DS} + V_T\right)\right]V_{DS} \quad (1)$$

where C_{ox} is the specific capacitance of the gate oxide, V_{DS} is the applied voltage of the drain electrode with respect to source electrode, and W and L are the channel width and length, respectively. V_T can provide valuable insight into the properties of the Si NC thin films, specifically with respect to the Fermi level.

The dependence of V_T on doping type and concentration was confirmed from the output characteristics, and typical output characteristics are shown in Figure 3 for large Si NCs. The expected saturation above the saturation voltage ($V_{SAT} = V_{GS} - V_T$) is evident for low nominally doped Si NCs and is marked by diamonds, where V_T was determined from the I_D−V_{GS} traces. For

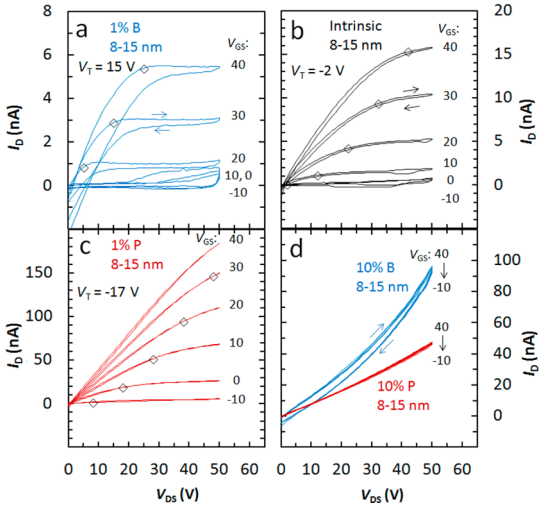

Figure 3. Output characteristics of Si NC thin-film transistors with nominally (a) 1% B-doped, (b) intrinsic, (c) 1% P-doped, and (d) 10% (blue) B- and (red) P-doped. Diamonds are where $V_{DS} = V_{SAT} = V_{GS} - V_T$, indicating the expected transition to saturation behavior, with V_T specified in each panel.

10% P- and B-doped Si NCs there is no gating behavior, which further confirms the degenerate doping.

In Figure 4a V_T is plotted as a function of nominal dopant concentration, and V_T is shown to be strongly dependent on the nominal doping type and concentration. Increasing the nominal doping concentration of B leads to higher positive V_T, and, conversely, higher concentrations of P lead to more negative V_T. The expected V_T for a FET can be calculated with the gradual channel approximation assuming bulk-like properties of the Si NC layer. A detailed description of this calculation and assumptions is provided in the Supporting Information. In Figure 4a the calculated V_T are shown for various dopant activation efficiencies η as a function of nominal doping concentration ($N_{a,nom}$), where the dopant activation efficiency η is defined as $N_{a,act} = \eta N_{a,nom}$, where $N_{a,act}$ is the actual extrinsic carrier density. A comparison between the experimental results and V_T predicted by the model reveals that B behaves as a p-type dopant that lowers the Fermi level, requiring higher positive gate voltages to accumulate charges in the channel, and P behaves as an n-type dopant that raises the Fermi level, as shown in the inset of Figure 4a. The efficiencies of dopant activation ($\sim 10^{-2}$–10^{-4}) are similar to EPR measurements of P-doped Si NCs synthesized using a different gas-phase synthesis method.[11] As Si NCs in that study were covered in a native oxide and defects at that Si/SiO_x interface may lead to dopant compensation, it is not obvious why the dopant activation efficiency is similar to our study, which is based on largely oxide-free Si NCs.

Size Dependence. In large NCs V_T changes over a large range as doping behavior shifts gradually between semiconducting and metallic-like, while for small P-doped NCs a sharp transition is observed from low off-currents (<1 nA) to high off-currents (10's of nA). This is evident in both the I_D–V_{GS} and output characteristics, as shown in Figure 5 (see Supporting Information Figure S5 for inclusion of small intrinsic and B doped). We attribute this behavior to the expected semidiscrete wave functions of Si NCs in films and the expected distribution of number of dopants in individual NCs. This distribution of dopants is expected to result in ensembles of NCs made of NCs that are either doped or intrinsic. This issue becomes especially evident for small NCs, where a small NC would be either intrinsic or degeneratively doped by a single active dopant. For example in a 4 nm Si NC, one active P dopant would result in a degenerative doping concentration of 3.13×10^{19} cm^{-3}, while for a large (12 nm) NC with one active P dopant, the doping concentration of 1.11×10^{18} cm^{-3} would be nearly degenerate and result in a V_T of −21 V in our device structure (assuming bulk-like properties). This binary nature of doping in small NCs leads to the observed increased off-currents due to conduction paths consisting of degenerate NCs along with additional gate-induced pathways of intrinsic NCs.

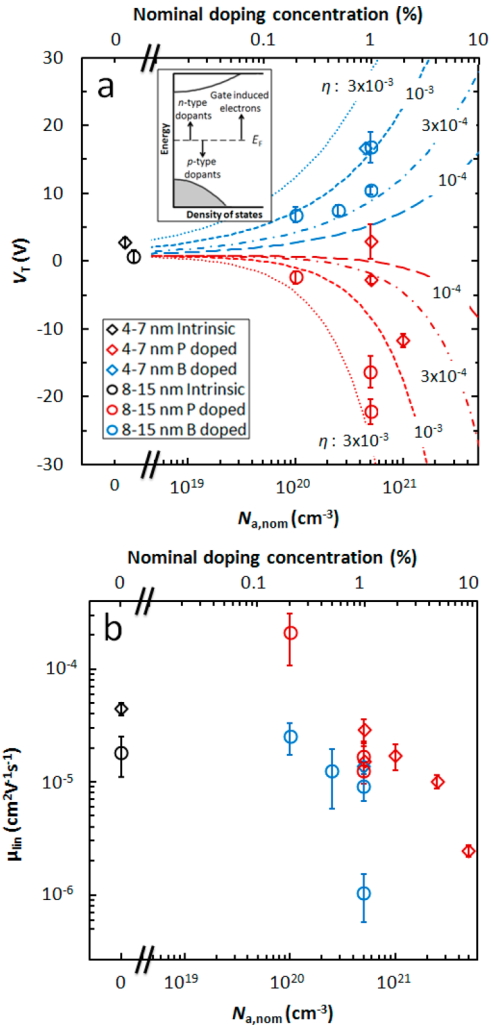

Figure 4. (a) Threshold voltage (V_T) summary as a function of nominal doping concentration and (b) μ_{lin} dependence on nominal doping concentration for (red) P, (black) intrinsic, and (blue) B Si NC thin films for (diamonds) small, 4–7 nm and (circles) large, 8–15 nm Si NC thin films. Error bars are the standard deviation of 5–8 devices fabricated from the same batch of NCs with at least two different substrates, where each point represents a different batch of NCs. Some points are slightly offset for clarity. Lines in (a) are calculated V_T for various active dopant activation efficiencies. Inset: Density of states diagram and the effect of dopants and gate-induced electrons on the Fermi level, E_F.

We assume the probability p_n of a single NC having n number of dopants follows Poisson statistics:

$$p_n = N_d{}^n/n! \exp(-N_d) \quad (2)$$

where N_d is the average number of active dopants per NC ($N_d = \eta N_{d,nom}(4/3\pi r^3 n_{si})$), η is taken from Figure 4a, and r is the average radius of the NC. For a small NC where one or more dopants result in a degenerate NC, the fractional concentration of degenerate NCs is given by $x = (1 - p_0)$.

According to percolation theory for a film made of a fraction of conducting (x) and insulating ($1 - x$) spheres, there is a percolation transition near a threshold x_c and the film is insulating below this value,

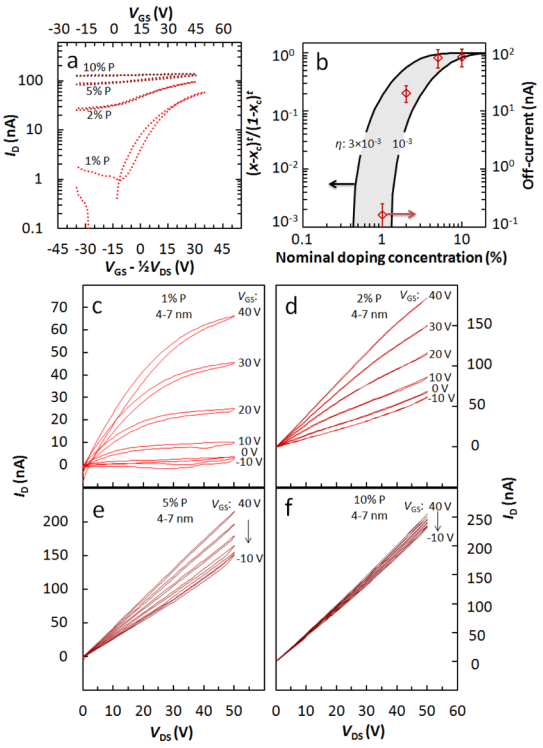

Figure 5. Characteristics of Si NC FETs fabricated with small (4−7 nm) Si NCs showing a sudden change from intrinsic to metallic behavior. (a) I_D-V_{GS} characteristics on a semilog scale, and (b) normalized scaling of conductivity according to percolation theory compared with the (steady-state) off-currents of 4−7 nm P-doped as a function of nominal doping concentration and output characteristics with nominally (c) 1% P-doped, (d) 2% P-doped, (e) 5% P-doped, and (f) 10% P-doped.

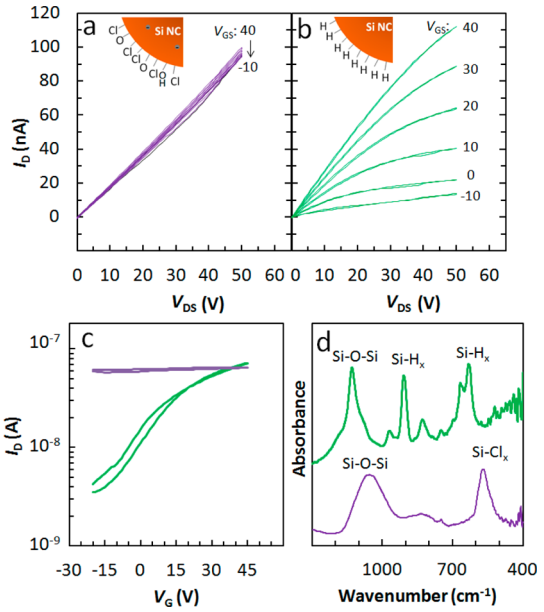

Figure 6. Output characteristics of (a) Si NC with chlorine termination and (b) after oxidation and HF etching; corresponding (c) I_D-V_{GS} characteristics and (d) FTIR for the same samples.

typically about 0.27.[25,26] Above this threshold the conductivity scales as $\sigma \propto (x - x_c)^t$, where t is in the range ~1.1−1.8, depending on a variety of factors including geometry, size dispersion, and packing of the film.[26] In Figure 5b the normalized scaling of conductivity $(x - x_c)^t/(1 - x_c)^t$ is compared to the off-current as a function of nominal doping concentration, where we assume a t of 1.73 and an r of 5 nm. The close agreement in trends between percolation theory and the experimental results supports the previous assumption that small NCs are either intrinsic or degenerate.

Influence of Surface. As the studies of chlorine-terminated Si NCs in ref 17 suggested the surprising surface doping of Si NCs through a Lewis acid−base interaction with a hard donor group of certain solvents (such as ketones and nitriles), we also investigated the properties of Cl-terminated Si NCs. As shown in Figure 6a, little to no gating behavior is observed, suggesting degenerate surface doping of the Si NCs. To further investigate if the surface of the NC was responsible for the minimal gating behavior, we intentionally oxidized the NCs and then etched the oxide with hydrofluoric acid (HF) vapor, resulting in a mostly hydrogen-terminated surface, as shown in Figure 6d. Once the chlorine was removed and replaced with hydrogen, the Si NCs demonstrated mobilities and gating behavior similar to Si NCs synthesized with hydrogen termination, as shown in Figure 6b.

These results suggest that one or more species at the surface add significant free carriers to the NCs with chlorine-terminated Si NCs. This apparent large number of free carriers for Si NCs with chlorine is supported by other experimental observations, such as our previous study on the optical extinction cross-section, where characteristics of free carrier absorption was observed in the infared.[27] Theoretical works predicted that chlorine-terminated Si NCs will have vastly different electronic properties compared to hydrogen-terminated Si NCs, where chlorine is expected to localize electrons near chlorine atoms (at the surface)[28] that act as electron trap states with the NCs expected to behave as good acceptors.[28−30] We suggest the degenerate behavior of Cl-terminated Si NCs arises from hard donor groups of organic solvents present in the glovebox atmosphere donating to the NC assisted by the presence of chlorine.

Mobility. A wide range of electron mobilities for the Si NC films, from $<10^{-6}$ to 5×10^{-4} cm^2 V^{-1} s^{-1} was found, with a summary of the size and dopant concentration dependence shown in Figure 4b. A general trend of decreasing mobility with increasing dopant concentration is apparent. This is likely responsible for the decrease in current observed for high nominally doped NCs compared to the on-current of less doped NCs (as shown in Figure 2). Films of small NCs along with P-doped NCs tended to have higher mobilities; however there was significant variation between batches of NCs made with identical synthesis conditions. Theoretical results predict a wide range of factors that influence the mobility in Si NC films including oxide thickness

between NCs, NC size and size distribution, and disorder in the packing structure.[31,32] Rigorous efforts were made to avoid oxidation in the samples examined in this study, and only minimal oxidation is evident as seen in typical FTIR spectra (shown in Figure S6). We can therefore exclude the influence of a large amount of oxide between NCs. However, a small amount of oxide may act as scattering centers, which reduces the mobility. Further investigation is necessary to elucidate the mobility-limiting mechanism.

All devices showed transport dominated by electrons, with the possible exception of those with 10% B doping. We attribute this electron-dominated transport to hole-type traps. However, ambipolar transport for several low B doped samples after annealing at 170 °C was observed, but the hole mobilities remained in the range of 10^{-6} cm^2 V^{-1} s^{-1}, and transient processes made it difficult to accurately determine device parameters.

CONCLUSIONS

In summary, the threshold voltage of Si NC FETs was found to be strongly dependent on dopant concentration and type, consistent with changes in the Fermi level of Si NC thin films caused by dopant activation with an efficiency of $\sim 10^{-2}$–10^{-4} of the nominal precursor concentration. Large NCs exhibited a continuum between intrinsic and degenerate doping, while small NCs show a sharp transition to degenerate doping, suggesting that the wave functions of NCs are still discrete. Additionally we found that chlorine-terminated Si NCs are doped through surface effects. These results reveal that both intentional inclusions of impurities in the core of Si NCs such as P and B and surface interactions can effectively dope Si NCs, resulting in control of the Fermi level and carrier concentration, which is desirable for the development of functional Si NC-based devices.

METHODS

Si NCs were synthesized in a nonthermal plasma as previously described,[10,18] where a continuous gas flow of silane or silicon tetrachloride and hydrogen,[19] argon, and, in the case of doped NCs, phosphine (15% in hydrogen) or diborane (10% in hydrogen) was introduced into a quartz reactor tube with power applied to ring electrodes.

Suspensions of Si NC "inks" were prepared by the addition of anhydrous 1,2-dichlorobenzene (Sigma-Aldrich) to dry Si NC powders with concentrations of about 2 mg mL^{-1}. Dispersions were formed by using a tip-ultrasonicator (Sonic & Materials, Inc., VCX130PB) at 25% power (resulting in ~2 W) for 1 min.

FETs were fabricated by successive spin-coating (1000 rpm) of Si NC dispersions onto cleaned doped (p+) silicon wafers with a 130 nm thermal oxide as the gate dielectric. While the thickness of the Si NC thin film scaled roughly linearly with the number of coatings, there was a significant batch-to-batch difference in the number of coatings required for similar thicknesses. The thickness of the thin film could be rationally estimated by its reflected color due to thin-film interference; a dark gold reflected color was used in this study, which corresponded to a thickness of about 10–40 nm, unless otherwise noted. Top aluminum contacts (60 nm) were thermally evaporated with a shadow mask with a width (W) of 2000 μm and a channel length (L) of 20 μm, unless otherwise noted.

FETs were measured at room temperature with a Keithley semiconductor characterization system (model SCS-4200) in a nitrogen-purified glovebox with oxygen and water concentrations of <1 ppm. The synthesis, handling, and measurements of FETs were performed without exposure to air.

ATR-FTIR spectroscopy (JASCO, 6100) was performed under vacuum with a ZnSe ATR crystal. Solutions of Si NCs in DCB were deposited onto the ATR crystal, and the analysis chamber was immediately evacuated with a roughing pump under a small flow of nitrogen gas and DCB was completely evaporated prior to acquiring spectra. The samples experienced a brief (<2 min) exposure to air, and the FTIR analysis was performed after device fabrication and characterization. Air-free FTIR spectroscopy of chlorine-terminated NCs was performed in a transmission mode air-free cell with thallium bromoiodide (KRS-5) windows with a layer of NCs deposited on one window.

SEM was performed with a JEOL-6700F, and TEM was performed on a FEI Tecnai G2 30 operating at 200 kV.

HF vapor etching (50% in water solution) of oxidized chlorine-terminated Si NCs was performed in a room-temperature container and allowed to progress slowly, requiring ~5 h to sufficiently etch the oxide on the Si NCs.

Conflict of Interest: The authors declare no competing financial interest.

Supporting Information Available: SEM images, XRD, detailed discussion of transient process in Si NC FETs, effect of film thickness on the on–off ratio, small NC device characteristics, threshold voltage calculations, and FTIR analysis. This material is available free of charge *via* the Internet at http://pubs.acs.org.

Acknowledgment. The work of R.G., D.Y., and T.N. was supported by the Funding Program for Next Generation World-Leading Researchers (GR040). R.G. was also partially supported by the Japanese Society for the Promotion of Science, Research Fellowship for Young Scientists (DC1). The work of N.J.K. and U.R.K. was supported by the DOE Plasma Science Center for Predictive Control of Plasma Kinetics. U.R.K. also acknowledges partial support by the Army Office of Research under MURI Grant W911NF-12-1-0407. T.C. is supported primarily by the National Science Foundation through the University of Minnesota MRSEC under Award Number DMR-0819885. Part of this work was carried out in the College of Science and Engineering Characterization Facility, University of Minnesota, which has received capital equipment funding from the NSF through the UMN MRSEC program. We thank K. Iwazumi for assistance with FTIR measurements.

REFERENCES AND NOTES

1. Cheng, K.-Y.; Anthony, R.; Kortshagen, U. R.; Holmes, R. J. High-Efficiency Silicon Nanocrystal Light-Emitting Devices. *Nano Lett.* **2011**, *11*, 1952–1956.
2. Nozik, A. J. Quantum Dot Solar Cells. *Phys. E Low-Dimens. Syst. Nanostruct.* **2002**, *14*, 115–120.
3. Erwin, S. C.; Zu, L.; Haftel, M. I.; Efros, A. L.; Kennedy, T. A.; Norris, D. J. Doping Semiconductor Nanocrystals. *Nature* **2005**, *436*, 91–94.
4. Norris, D. J.; Efros, A. L.; Erwin, S. C. Doped Nanocrystals. *Science* **2008**, *319*, 1776–1779.
5. Sahu, A.; Kang, M. S.; Kompch, A.; Notthoff, C.; Wills, A. W.; Deng, D.; Winterer, M.; Frisbie, C. D.; Norris, D. J. Electronic Impurity Doping in CdSe Nanocrystals. *Nano Lett.* **2012**, *12*, 2587–2594.
6. Wills, A. W.; Kang, M. S.; Wentz, K. M.; Hayes, S. E.; Sahu, A.; Gladfelter, W. L.; Norris, D. J. Synthesis and Characterization of Al- and In-Doped CdSe Nanocrystals. *J. Mater. Chem.* **2012**, *22*, 6335–6342.

7. Kim, D. K.; Fafarman, A. T.; Diroll, B. T.; Chan, S. H.; Gordon, T. R.; Murray, C. B.; Kagan, C. R. Solution-Based Stoichiometric Control over Charge Transport in Nanocrystalline CdSe Devices. *ACS Nano* **2013**, *7*, 8760–8770.
8. Kang, M. S.; Sahu, A.; Frisbie, C. D.; Norris, D. J. Influence of Silver Doping on Electron Transport in Thin Films of PbSe Nanocrystals. *Adv. Mater.* **2013**, *25*, 725–731.
9. Oh, S. J.; Berry, N. E.; Choi, J.-H.; Gaulding, E. A.; Paik, T.; Hong, S.-H.; Murray, C. B.; Kagan, C. R. Stoichiometric Control of Lead Chalcogenide Nanocrystal Solids to Enhance Their Electronic and Optoelectronic Device Performance. *ACS Nano* **2013**, *7*, 2413–2421.
10. Pi, X. D.; Gresback, R.; Liptak, R. W.; Campbell, S. A.; Kortshagen, U. Doping Efficiency, Dopant Location, and Oxidation of Si Nanocrystals. *Appl. Phys. Lett.* **2008**, *92*, 123102–3.
11. Stegner, A. R.; Pereira, R. N.; Lechner, R.; Klein, K.; Wiggers, H.; Stutzmann, M.; Brandt, M. S. Doping Efficiency in Freestanding Silicon Nanocrystals from the Gas Phase: Phosphorus Incorporation and Defect-Induced Compensation. *Phys. Rev. B* **2009**, *80*, 165326.
12. Rowe, D. J.; Jeong, J. S.; Mkhoyan, K. A.; Kortshagen, U. R. Phosphorus-Doped Silicon Nanocrystals Exhibiting Mid-Infrared Localized Surface Plasmon Resonance. *Nano Lett.* **2013**, *13*, 1317–1322.
13. Talapin, D. V.; Murray, C. B. PbSe Nanocrystal Solids for n- and p-Channel Thin Film Field-Effect Transistors. *Science* **2005**, *310*, 86–89.
14. Zhou, X.; Uchida, K.; Mizuta, H.; Oda, S. Electron Transport in Surface Oxidized Si Nanocrystal Ensembles with Thin Film Transistor Structure. *J. Appl. Phys.* **2009**, *106*, 044511.
15. Holman, Z. C.; Liu, C.-Y.; Kortshagen, U. R. Germanium and Silicon Nanocrystal Thin-Film Field-Effect Transistors from Solution. *Nano Lett.* **2010**, *10*, 2661–2666.
16. Weis, S.; Körmer, R.; Jank, M. P. M.; Lemberger, M.; Otto, M.; Ryssel, H.; Peukert, W.; Frey, L. Conduction Mechanisms and Environmental Sensitivity of Solution-Processed Silicon Nanoparticle Layers for Thin-Film Transistors. *Small* **2011**, *7*, 2853–2857.
17. Wheeler, L. M.; Neale, N. R.; Chen, T.; Kortshagen, U. R. Hypervalent Surface Interactions for Colloidal Stability and Doping of Silicon Nanocrystals. *Nat. Commun.* **2013**, 4.
18. Mangolini, L.; Thimsen, E.; Kortshagen, U. High-Yield Plasma Synthesis of Luminescent Silicon Nanocrystals. *Nano Lett.* **2005**, *5*, 655–659.
19. Gresback, R.; Nozaki, T.; Okazaki, K. Synthesis and Oxidation of Luminescent Silicon Nanocrystals from Silicon Tetrachloride by Very High Frequency Nonthermal Plasma. *Nanotechnology* **2011**, *22*, 305605.
20. Luther, J. M.; Law, M.; Song, Q.; Perkins, C. L.; Beard, M. C.; Nozik, A. J. Structural, Optical, and Electrical Properties of Self-Assembled Films of PbSe Nanocrystals Treated with 1,2-Ethanedithiol. *ACS Nano* **2008**, *2*, 271–280.
21. Liu, Y.; Gibbs, M.; Puthussery, J.; Gaik, S.; Ihly, R.; Hillhouse, H. W.; Law, M. Dependence of Carrier Mobility on Nanocrystal Size and Ligand Length in PbSe Nanocrystal Solids. *Nano Lett.* **2010**, *10*, 1960–1969.
22. Powell, M. J.; Deane, S. C.; Milne, W. I. Bias-Stress-Induced Creation and Removal of Dangling-Bond States in Amorphous Silicon Thin-Film Transistors. *Appl. Phys. Lett.* **1992**, *60*, 207–209.
23. Deane, S. C.; Wehrspohn, R. B.; Powell, M. J. Unification of the Time and Temperature Dependence of Dangling-Bond-Defect Creation and Removal in Amorphous-Silicon Thin-Film Transistors. *Phys. Rev. B* **1998**, *58*, 12625–12628.
24. Sze, S. M.; Ng, K. K. *Physics of Semiconductor Devices*; John Wiley & Sons, 2006.
25. Efros, A. L.; Shklovskii, B. I. Critical Behaviour of Conductivity and Dielectric Constant near the Metal-Non-Metal Transition Threshold. *Phys. Status Solidi B* **1976**, *76*, 475–485.
26. Clerc, J. P.; Giraud, G.; Alexander, S.; Guyon, E. Conductivity of a Mixture of Conducting and Insulating Grains: Dimensionality Effects. *Phys. Rev. B* **1980**, *22*, 2489–2494.
27. Gresback, R.; Murakami, Y.; Ding, Y.; Yamada, R.; Okazaki, K.; Nozaki, T. Optical Extinction Spectra of Silicon Nanocrystals: Size Dependence upon the Lowest Direct Transition. *Langmuir* **2013**, *29*, 1802–1807.
28. Carvalho, A.; Öberg, S.; Rayson, M. J.; Briddon, P. R. Electronic Properties, Doping, and Defects in Chlorinated Silicon Nanocrystals. *Phys. Rev. B* **2012**, *86*, 045308.
29. Ma, Y.; Chen, X.; Pi, X.; Yang, D. Theoretical Study of Chlorine for Silicon Nanocrystals. *J. Phys. Chem. C* **2011**, *115*, 12822–12825.
30. Martínez, A.; Alonso, J. C.; Sansores, L. E.; Salcedo, R. Electronic Structure of Silicon Nanocrystals Passivated with Nitrogen and Chlorine. *J. Phys. Chem. C* **2010**, *114*, 12427–12431.
31. Lepage, H.; Kaminski-Cachopo, A.; Poncet, A.; le Carval, G. Simulation of Electronic Transport in Silicon Nanocrystal Solids. *J. Phys. Chem. C* **2012**, *116*, 10873–10880.
32. Seino, K.; Bechstedt, F.; Kroll, P. Tunneling of Electrons between Si Nanocrystals Embedded in a SiO_2 Matrix. *Phys. Rev. B* **2012**, *86*, 075312.